Journal of Volcanology and Geothermal Research 443 (2023) 107930

Contents lists available at ScienceDirect

Journal of Volcanology and Geothermal Research

journal homepage: www.journals.elsevier.com/journal-of-volcanology-and-geothermal-research

The effects of hot and pressurized fluid flow across a brittle layer on the recent seismicity and deformation in the Campi Flegrei caldera (Italy)

Massimo Nespoli [a,*], Anna Tramelli [b], Maria Elina Belardinelli [a], Maurizio Bonafede [a]

[a] Department of Physics and Astronomy, Alma Mater Studiorum, Università di Bologna, Viale Berti Pichat 6/2, Bologna, Italy
[b] Istituto Nazionale di Geofisica e Vulcanologia, Sezione di Napoli, Osservatorio Vesuviano, Via Diocleziano 328, 80124, Napoli, Italy

ARTICLE INFO

Original content: Seismic Catalog of Campi Flegrei (Original data)

Keywords:
Campi Flegrei
Hydrothermal fluids
Caldera
Uplift
Induced seismicity
Deformation source

ABSTRACT

The influence of the hydrothermal circulation on seismicity and uplift observed at the Campi Flegrei caldera (Italy) is a topic of great interest to the scientific community. Recently, Thermo-Poro-Elastic (TPE) inclusions were proposed as likely deformation sources. They are suitable to explain the mechanical effects induced by hot and pressurized hydrothermal fluids, possibly exsolved from underlying magma, and pervading an overlying brittle layer. Recent works show that a TPE inclusion located at approximately 2 km depth below the Campi Flegrei caldera significantly contributed to the large and rapid soil uplift observed during the '82-'84 unrest phase. In the present work we demonstrate that such a source of deformation is likely playing a role even in the current unrest phase, which is characterized by a much lower uplift-rate with respect to the one occurred in the previous unrest phase. We will show that the time-series of soil uplift observed in the last 18 years can be reproduced by assuming the reactivation of the same deformation source responsible of the '82-'84 unrest located within a shallow brittle layer at about 2 km depth. The presence of a brittle layer has been evidenced in the past by tomographic studies and is confirmed by a sharp variation of the b-value at the corresponding depth. We believe that our results provide very important insights and evidences, supporting the existence and the importance of an active thermo-poro-elastic deformation source, which can be useful for understanding the unrest of the Campi Flegrei caldera, from both a scientific and geohazard perspective.

1. Introduction

The Campi Flegrei caldera (Fig. 1) is located west of the city of Naples (Italy). This area experiences volcanic activity since at least 47,000 years ago (De Vivo, 2006). The two major eruptive episodes occurred about 39,000 and 14,900 years BP,while the last eruption occurred in 1538 AD. From the middle of the last century the caldera has experienced several episodes of uplift and subsidence (e.g. Di Vito et al., 1999). The area is also characterized by shallow seismicity (Tramelli et al., 2022), which is generally low in magnitude (few events up to Md = 4.0). Two important unrest phases occurred in 1969–1972 and 1982–1984. During the 1982–1984 bradyseismic crisis, the maximum measured uplift was of almost 1.8 m and it was accompanied by >16,000 earthquakes. After 1984, the caldera experienced a 20 years long phase of subsidence occasionally interrupted by small and short uplift episodes. In 2000 the uplift rate slightly reversed and in 2005 a new uplift phase clearly began (Bevilacqua et al., 2022). Since 2000, also the seismicity rate increased with time, especially onshore below the area of the Solfatara crater.

According to the literature, the uplift episodes can be partly due to the fluid flow of the shallow hydrothermal system and partly to the magma emplacement and movement (Berrino, 1994; Battaglia et al., 2006; Chiodini et al., 2021, 2015; Mantiloni et al., 2020; Nespoli et al., 2021; Todesco, 2021; Trasatti et al., 2011). Even if the presence of significant magmatic bodies in the shallowest 2 km of depth was excluded by the seismic tomographies (Judenherc and Zollo, 2004) and by analysis of deep drilling geophysical data (Carlino et al., 2012). For example, the uplift observed during the '82-'84 unrest phase was efficiently modelled with both a magma filled dislocation source located at 4.5 km depth (Trasatti et al., 2011) and a sill intrusion at about 3 km depth (D'Auria et al., 2015). Amoruso et al. (2007) showed that even the deformation observed during the 2004–2006 period can be satisfactory explained adopting a horizontal circular crack located at 3.5 km of depth, with a radius of 2.5 km. However, hydrothermal deformation sources can be considered as well. For example, De Natale et al. (2001) suggested that, during the '82-'84 unrest period, the fluid flow caused by

* Corresponding author.
E-mail address: massimo.nespoli2@unibo.it (M. Nespoli).

https://doi.org/10.1016/j.jvolgeores.2023.107930
Received 23 May 2023; Received in revised form 5 October 2023; Accepted 8 October 2023
Available online 12 October 2023

an increase of pressure and/or temperature at depth, had significant role in inducing ground movements in the Campi Felgrei caldera. Bianco et al. (2004) found that even the seismic swarm occurred in 2000 was associated to the rising of a pressure front triggered by an excess of fluid pressure released by a magmatic intrusion.

According to Tramelli et al. (2022) the space-time evolution of recent seismic swarms is well explained by fluid injection from a deeper magma source. This evidences an analogy with the 1982–84 crises when, according to Thermo-Poro-Elastic (TPE) models (e.g. Mantiloni et al., 2020; Nespoli et al., 2021), the seismicity was induced by the deformation (and stress) due to the TPE response of a shallow volume (inclusion) filled up by hot and pressurized fluids released from a deeper magma reservoir. The existence of such a volume was evidenced by tomographic studies (e.g. Calò and Tramelli, 2018) performed using the earthquakes recorded during the 1982–84 crises. The geometry and location of the TPE source was retrieved by Nespoli et al. (2021) by inverting the deformation data measured during the 1982–1984 unrest phase, considering a layered crustal model. According to their results, the TPE source is traceable as a flat cylinder (width = 500 m, radius = 2550 m) located at 1875 m of depth (Fig. 1). While such a source of deformation was successfully applied to model the 1982–1984 unrest, to date, it has not yet been applied to the most recent seismicity and deformation.

The focus of the present work is therefore to investigate if, and how much, the recent deformation and seismicity of Campi Flegrei can be explained by reactivation of the same source of deformation employed by Mantiloni et al. (2020) and Nespoli et al. (2021) to model the 1982–1984 unrest. This assumption is consistent with a scenario in which the TPE source acts as a valve, which episodically allows or prevents the rising of hot and pressurized fluids exsolved from a deeper magma chamber (Calò and Tramelli, 2018; Lima et al., 2021; Nespoli et al., 2021). The 1982–84 and the currently ongoing unrests may represent stages during which rising of fluids is allowed, while the period 1984–2005 can be interpreted as a phase of much more reduced fluid flow. While previous works used the TPE inclusions to model a static deformation pattern, in the present work we will show, for the first time, how to model transient deformation patterns.

In the next section we analyse the b-value of the recent seismic catalog (from 2000 to the middle of 2022). We find a sharp decrease below ≈ 1.5 km of depth (Fig. 2), where the TPE source is expected to be located according to Nespoli et al. (2021). A strong reduction of the b-value with depth was already found by Vilardo et al. (1991) who analysed the seismic catalog of earthquakes occurred in the 1983–1984 period. This evidence supports the hypothesis that there may be different failure conditions at different depths in the Campi Flegrei caldera, as we shall argue in the discussion section.

2. Material and methods

2.1. Analysis of the b-value

The b-value describes the frequency-magnitude distribution of earthquakes, with values that are around unity. Seismological observations and laboratory experiments inferred that the b-value varies with differential stress, faulting style mechanisms, earthquake depth, plate tectonics and temperature (e.g. Wyss et al., 1997; Wiemer and Wyss,

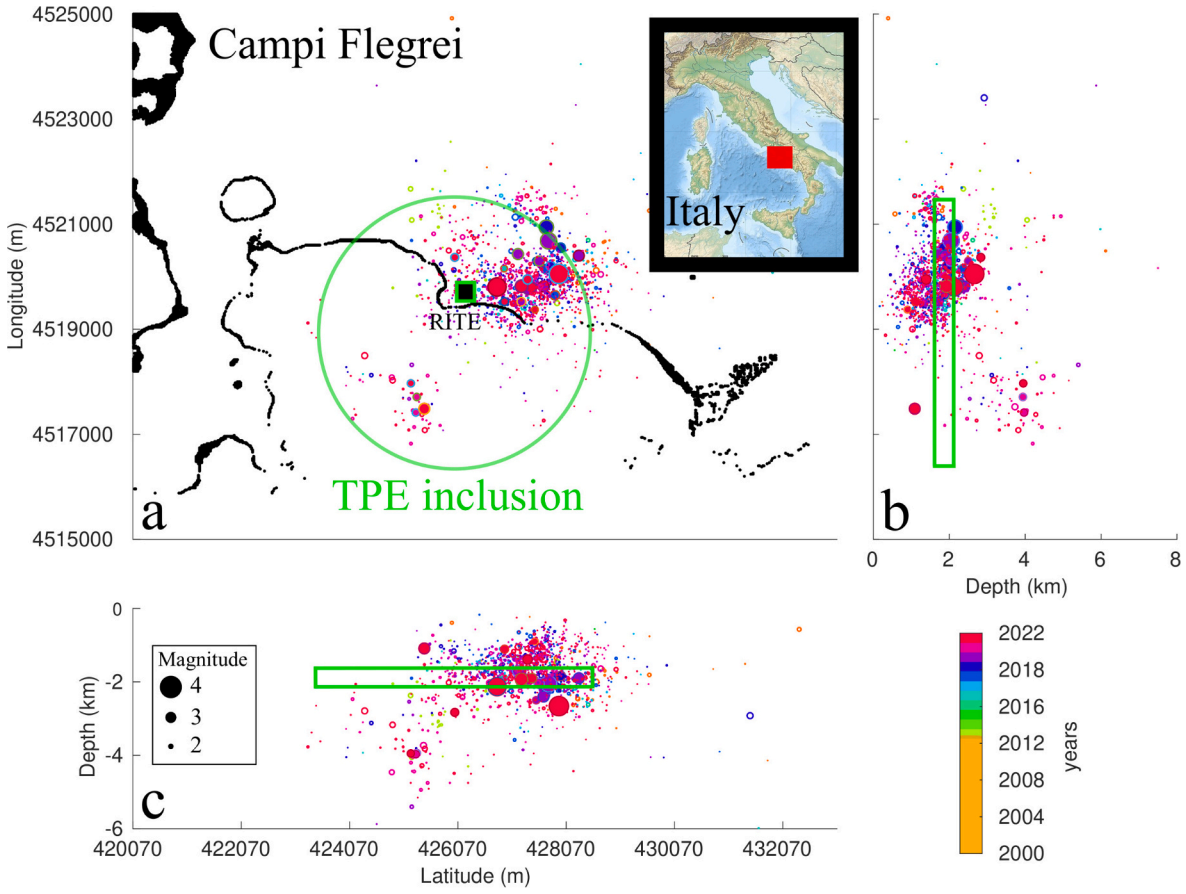

Fig. 1. Relocated hypocenters (points) of earthquakes occurred between 2000 and 2022 at Campi Flegrei in map (a) and vertical sections (b, c). The size of the circles is proportional to the magnitude of the earthquakes. The black square indicates the location of the RITE CGNSS station. The green lines indicate the boundaries of the TPE inclusion, as retrieved by Nespoli et al. (2021) from the inversion of geodetic data measured during the period June 1980–June 1983 (width = 500 m, radius = 2550 m, depth 1875). (For interpretation of the references to colour in this figure legend, the reader is referred to the web version of this article.)

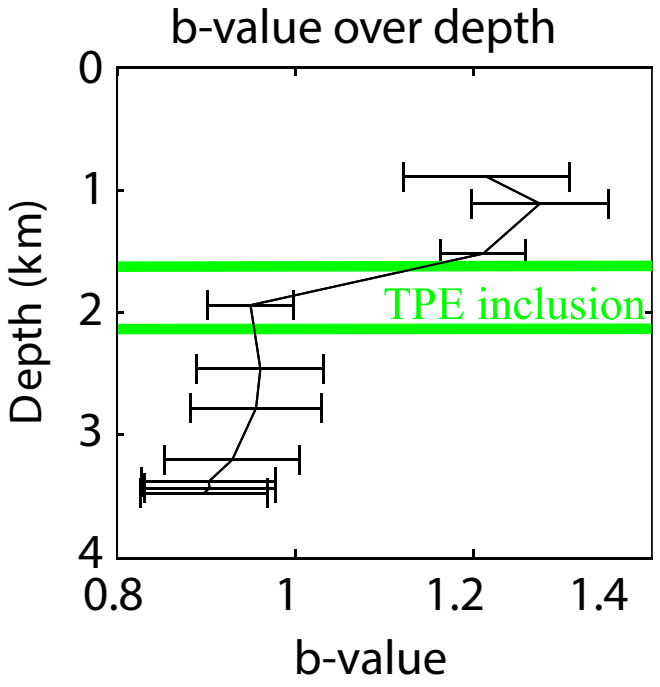

Fig. 2. Computed b-value as a function of depth. The green lines indicate the location of the top and the bottom boundaries of the TPE inclusion, as retrieved by Nespoli et al. (2021). (For interpretation of the references to colour in this figure legend, the reader is referred to the web version of this article.)

2002; Schorlemmer et al., 2005). Moreover, according to the fractal theories of seismicity (e.g. Turcotte, 1989) greater b-values are associated to a statistical distribution of characteristic faults dominated by smaller geometrical dimensions (i.e. to a more intense fragmentation of the focal volume).

We analysed the b-value variations with depth to evidence any anomaly that can be related to temperature, rheological or stress heterogeneities. For this analysis we considered the 2000–2022 Campi Flegrei seismic catalog compiled by INGV-Osservatorio Vesuviano and relocated employing the 3D velocity model of D'Auria et al. (2008). We used a completeness magnitude (the magnitude above which each earthquake is present in the catalog) of 0.4 (the more conservative value found by Tramelli et al., 2021). For each depth interval, we considered the closest 150 earthquakes and estimated the b-value using the maximum likelihood method (Aki, 1965). The uncertainty is estimated using the Shi and Bolt (1982) formula. The number of earthquakes (1332 with Md $\geq$ 0.4 since 2005) and their location (most of them are located in a small volume below Solfatara/Pisciarelli; see Fig. 1) don't allow to perform a 3D spatial analysis of the b-value.

In Fig. 2 we report the obtained results. The b-value of Campi Flegrei decreases with increasing depth from 1.3 to 0.9. A sharp variation of the b-value is clearly visible from about 1.5 km to about 2 km depth.

2.2. The TPE model

We model the time series uplift measured at the RITE CGNSS station (Fig. 4a and 5) during the time interval 2000–2022 (De Martino et al., 2021) in terms of evolving temperature and pore-pressure inside the TPE inclusion. RITE station (Fig. 1) is located near the centre of the caldera where the maximum uplift is measured. At the Campi Flegrei caldera the geometrical pattern of the normalized displacement field is nearly constant over time (e.g. Vitale and Natale, 2023), so that the RITE station time history actually constrains the whole deformation pattern (Fig. 3).

Both displacement and stress due to a TPE inclusion linearly depend on the potency e_0 (Belardinelli et al., 2019; Nespoli et al., 2021):

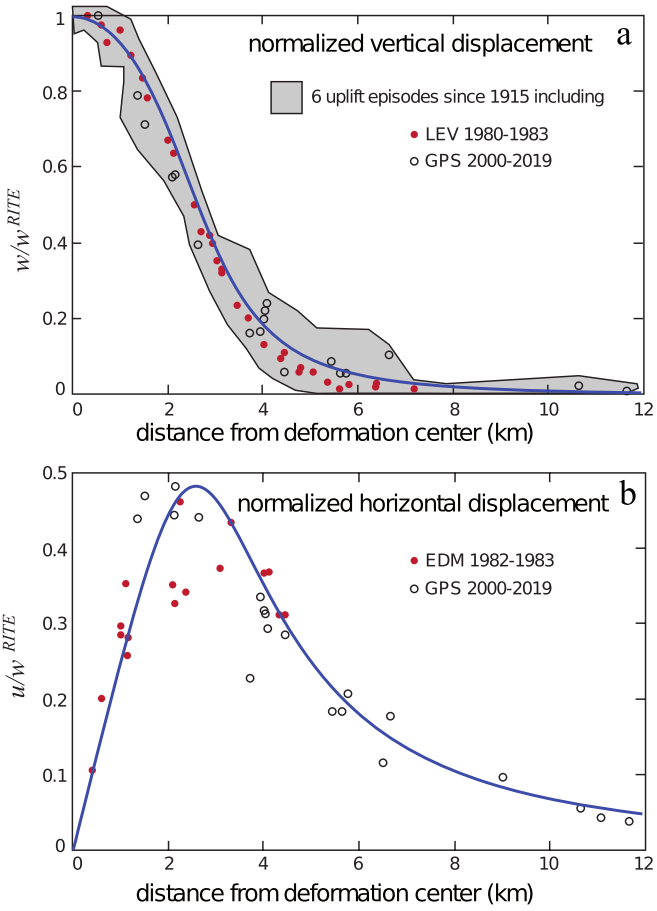

Fig. 3. Normalized displacement as a function of the distance from the deformation centre, measured during different uplift episodes occurred in the Campi Flegrei Caldera, (a) Data of vertical displacements obtained with levelling (Amoruso et al., 2014) during the period 1980–1983 (red points), with GPS during the 2000–2019 period (black circles) and during 6 different uplift episodes occurred since 1915 (gray area). (b) Data of horizontal displacements obtained with electromagnetic distance measurement (EDM) (Amoruso et al., 2014) during the period 1980–1983 (red points) and with GPS (De Martino et al., 2021) during the 2000–2019 period (black circles). The blue curves represent the displacement computed with the TPE inclusion considered in the present work. (For interpretation of the references to colour in this figure legend, the reader is referred to the web version of this article.)

$$e_0 = \frac{1}{3H}p + \frac{1}{3}\alpha_s T \quad (1)$$

which, in turn, linearly depends on changes of temperature T and pore pressure p, with respect to an initial reference state. In eq. (1) H is a poroelastic parameter as introduced by Biot (1941) and α_s is the thermal expansion coefficient of the solid matrix of the poroelastic medium.

The displacement field produced by T and p changes can be computed following the Eshelby (1957) inclusion method. Briefly, this method consists in:

- ideally extracting the volume destined to experience T and p changes (the inclusion) from the embedding medium (kept in equilibrium by applying suitable artificial tractions $\tau_{ij}^{(A)}$ over the resulting cavity surface S); by definition, the embedding medium remains at constant temperature and pressure.
- heating and pressurizing the inclusion under free-boundary conditions; the inclusion suffers an isotropic "free strain" $e_0\,\delta_{ij}$;
- straining the inclusion to the initial volume by applying artificial tractions $\tau_{ij}^{(B)}$ over the surface of the inclusion;

- inserting the inclusion back inside the embedding medium: a traction discontinuity is now present on *S;*
- finally, the displacement is computed at any point of the medium by applying an opposite traction discontinuity on *S* (e.g. Aki and Richards, 2002) in order to restore traction continuity.

For a given potency e_0, the displacement field in **x** is then given by:

$$u_i(\mathrm{x}) = 3Ke_0 \int_S G_{ik}(\mathrm{x}, \mathrm{x}')n_k(\mathrm{x}')dS' \tag{2}$$

where G_{ik} (**x**, **x**') is the elastic Green's tensor for a half-space (representing the displacement in **x** due to a unitary force located in **x**'), K the drained isothermal bulk modulus and S the surface embedding the inclusion.

The equations for the vertical propagation of pore-pressure and temperature inside a disk-shaped TPE inclusion, due to the input of fluids inducing changes of Δp and ΔT at the base of the inclusion ($z = 0$), were obtained by Nespoli et al. (2021) and Belardinelli et al. (2022). Considering a fluid phase (subscript *f*) moving within a solid matrix $0 \leq z \leq b$ (subscript *s*) represented with TPE parameters reported in Table 1, the approximate solution for temperature can be obtained by imposing the energy balance of the system (Bejan, 1984) and neglecting heat conduction compared with advection processes (Nespoli et al., 2021):

$$T(z,t) = \Delta T[1 - \theta(z - V_T t)] \tag{3}$$

where $\Theta(x)$ is the Heaviside step function ($\Theta(x) = 0$ if $x < 0$, $\Theta(x) = 1$ if $x > 0$), z denotes the vertical coordinate and V_T is the speed of the temperature front

$$V_T = \frac{\rho_f c_f}{\phi\rho_f c_f + (1-\phi)\rho_s c_s} q \tag{4}$$

which depends on the Darcy's velocity in vectorial form:

$$\mathbf{q} = -\frac{k}{\eta}\nabla p \tag{5}$$

In the eqs. (4) and (5) ρ is the density, c is the specific heat, ϕ is the porosity, k is the permeability and η is the fluid viscosity.

Solution (3) for the temperature is obtained by neglecting conduction and using for the pressure (which governs the advective process) a preliminary solution $p^{(0)}(z) = \Delta p(1\text{-}z/b)$, with constant gradient which ignores the interaction between p and T within the inclusion $0 \leq z \leq b$. The quasi-static solution for the pore-pressure computed between the base ($z = 0$) and the top ($z = b$) of the inclusion can be obtained imposing the fluid mass conservation and the compatibility equations (McTigue, 1986) and can be computed following Nespoli et al. (2021) and Belardinelli et al. (2022) assuming the solution (3) for T as:

$$p(z,t) = \begin{cases} \Delta p\left(1 - \frac{z}{b}\right) + \Gamma z\left(1 - V_T\frac{t}{b}\right) \text{ if } 0 \leq z \leq V_T t \\ (\Delta p + \Gamma V_T t)\left(1 - \frac{z}{b}\right) \text{ if } V_T t < z \leq b, \end{cases} \tag{6}$$

where

$$\Gamma = \frac{(\gamma_1 + \gamma_2)V_T \Delta T}{D}$$

$$\gamma_1 = \frac{4}{9}\mu B \alpha_s \frac{(1+\nu_u)}{(1-\nu_u)}$$

$$\gamma_2 = \frac{2}{9}\mu B^2 \phi(\alpha_f - \alpha_s)\frac{(1-\nu)(1+\nu_u)^2}{(1-\nu_u)(\nu_u - \nu)}$$

with

$$D = \frac{k\mu}{\eta}\frac{2B^2(1+\nu_u)^2(1-\nu)}{9(1-\nu_u)(\nu_u - \nu)},$$

μ is the rigidity, B is the Skempton's coefficient, α is the thermal expansion, ν_u is the undrained Poisson's ratio. D is the hydraulic diffusivity. The procedure might be iterated to find a new solution for T that employs the solution (6) for p to describe thermal advection; however, for realistic values of ΔT ($<10^3$ K) the two different gradients of p in (6), before and after $z = V_T t$ do not differ appreciably from each other so that (3) is assumed a reasonable approximation of the exact solution. We stress that the material embedding the inclusion is assumed elastic, endowed with the same free-drainage elastic constants as the inclusion. In principle, the embedding medium is not affected by p and T changes because these changes by definition, take place inside the inclusion, whose volume is not necessarily fixed "a priori". However, for simplicity sake, the pressure solution (6) is obtained assuming a fixed dimension for the inclusion and, as a consequence, even the solution (3) for T depends from this assumption since the T front is not fixed, but advances with velocity V_T which depends on p. A fixed inclusion dimension may be justified envisaging a scenario in which the medium overlying the inclusion is endowed with high permeability and is affected by enhanced meteoric flows able to maintain nearly constant T and p.

The provided solutions are reliable to model the effects of hot and pressurized fluids rising from the bottom of the TPE region toward the surface, under the simplified assumptions of pure vertical propagation of fluids in isothermal and hydrostatic initial conditions and constant high permeability. The assumption of high permeability is consistent with a fractured medium, as it is expected to be in the interior of the TPE inclusion. Such an assumption allows neglecting the heat conduction occurring across the lateral boundaries of the TPE inclusion where only conductive heat transfer may apply, which is negligible compared to vertical advective transfer (Nespoli et al., 2021; Belardinelli et al., 2022). The solution for the T profile (3), represents the effects of a thermal front rising from the bottom of the inclusion with a constant velocity V_T. As V_T depends on the Darcy's velocity (5), larger pore pressure gradients lead to faster thermal fronts and vice-versa. The p profile (6) consists in two rectilinear segments, with uniform gradients, which slowly vary with time. The two segments match to each other continuously at the depth of the rising thermal front $z = V_T t$. Unless in case of a low permeability, such a configuration for pore-pressure is reached very quickly with respect to the time required by the thermal front to rise upward (Belardinelli et al., 2022).

Differently from previous applications of TPE inclusions, which assume a static deformation pattern, we want to find a procedure to model the variations of displacement and seismicity over time. To model transient mechanical effects due to the fluid propagation inside the inclusion according to (3) and (6), a TPE inclusion (Fig. 1) with the same

Table 1
Thermo-Poro-Elastic parameters of eqs. 3 and 6. Subscripts *s* and *f* refer to the solid and fluid phase, respectively. The parameters represent a quite competent and porous material (Table 1, Wang, 2017) permeated by a water substance.

Symbol	Parameter	Unit of measure	Value
ρ_s	Density of solid	Kg/m^3	2650
ρ_f	Density of fluid	Kg/m^3	1000
Φ	Porosity	–	0.2
c_s	Specific heat of solid	J/(kg · K)	1000
c_f	Specific heat of fluid	J/(kg · K)	4200
B	Skempton parameter	–	0.62
α_s	Thermal expansion of solid	1/K	$3 \cdot 10^{-5}$
α_f	Thermal expansion of fluid	1/K	$5 \cdot 10^{-4}$
μ	Shear modulus	Pa	$6 \cdot 10^{9}$
ν_u	Undrained Poisson's ratio	–	0.2
η	Fluid viscosity	Pa·s	$1 \cdot 10^{-3}$
H	Poro-elastic parameter	Pa	$1.01 \cdot 10^{10}$
k_{C1}	Permeability of C1	m^2	$1.9 \cdot 10^{-12}$
k_{C2}	Permeability of C2	m^2	$1.9 \cdot 10^{-13}$
k_{C3}	Permeability of C3	m^2	$1.9 \cdot 10^{-14}$
k_{C4}	Permeability of C4	m^2	$1.9 \cdot 10^{-15}$

geometry as the one retrieved by Nespoli et al. (2021) was represented by a vertical superposition of 100 disk-like slices (e.g. Benussi et al., 2023). We first evaluate the effect of each slice on both deformation and stress field assuming a unitary TPE potency, e_0, inside it. Following this procedure, we can compute a sort of Green's functions for each slice of the TPE inclusion. By summing the effects of the slides located at z multiplied by e_0 (eq. 1) with $p(z,t)$ and $T(z,t)$, according to (3) and (6), we can model the effects of the vertical distribution of pressure and temperature for a given time t after the beginning of the exsolution of fluids inside the inclusion. Both deformation and stress were computed with the *EFGRN/EFCMP* software (Nespoli et al., 2022) which allows us to compute the mechanical effects of a TPE inclusion with an arbitrary shape. This can be done by representing the inclusion with a distribution of single forces acting normally on its surface (Nespoli et al., 2022), according to (2). To keep coherence between the several parameters describing the solid and fluid phase, we assume uniform parameters for all slices, as reported in Table 1. A direct estimate of all the poro-elastic parameters that characterize the study area is not available. However, the used parameters are suitable to represent a quite competent and porous material (Table 1, Wang, 2017) permeated by a water substance and are consistent with previous studies (e.g. Belardinelli et al., 2022; Nespoli et al., 2021). The used permeability values are compatible with the range measured by Heap et al. (2014) in the study area. The assumption of a water substance for fluids is an approximation which is in agreement with the 3D model of the electrical resistivity by Troiano et al. (2022) who suggested the influx of hot fluids of magmatic origin, prevalently in the liquid phase, at about 2 km of depth, which corresponds to the depth of the bottom of the TPE inclusion.

In order to model the knee point of the time series of the uplift measured at the RITE station in ≈2012 (Fig. 4a), we assumed that the pore pressure of the fluids at the base of the TPE source changed abruptly between 2011 and 2012 and at the beginning of 2020 ($\Delta p = \Delta p_1$ for $t <$ 06/2011; $\Delta p = \Delta p_2$ for 06/2011 $\leq t <$ 01/2020 and $\Delta p = \Delta p_3$ for $t \geq$ 01/2020). The three different Δp values allow us to represent a piecewise-constant function describing the evolution of increasing pore-pressure at the base of the inclusion. In this way we can reproduce the increase over time of the uplift rate as due to the arrival of three different plumes of fluids. Instead, the temperature of fluids at the base of the TPE inclusion is assumed constant since it is controlled by thermal conditions of the underlying region. The increment in the fumarolic CO/CO_2 ratio with time reported by Chiodini et al. (2015) and Tramelli et al. (2021) also suggested an ongoing heating and pressurization due to the fluids rising in the same periods. Such a scenario seems reasonable because the time series of the uplift measured at Campi Flegrei during the considered time-windows can be well approximated with two linear trends, before and after the middle of 2011 (Tramelli et al., 2021) and a third one after 2020 (Fig. 4a).

3. Simulations and results

In order to study the effects of fluid injection into the TPE inclusion, we consider 4 different cases (C1 to C4). All cases represent an injection of hot and pressurized fluids, considering four different permeability values (C1 to C4: $k_{C1} = 1.9{\cdot}10^{-12}$ m^2, $k_{C2} = 1.9{\cdot}10^{-13}$ m^2, $k_{C3} = 1.9{\cdot}10^{-14}$ m^2, $k_{C4} = 1.9{\cdot}10^{-15}$ m^2). The parametric study of permeability values is recommended since reasonable values of rock permeability span over several orders of magnitude (e.g. Wang, 2017). For each case, we found the best temperature (ΔT) and pore-pressure changes (Δp_1, Δp_2 and Δp_3) describing the boundary condition for p at the base of the inclusion in terms of a step-wise increasing function of time, which allow us to reproduce the time series of vertical displacement measured at the RITE CGNSS station. The search for the best fit parameters were performed using a Monte-Carlo sampling with a direct parameter search. The best parameters are then chosen as the ones having the greater

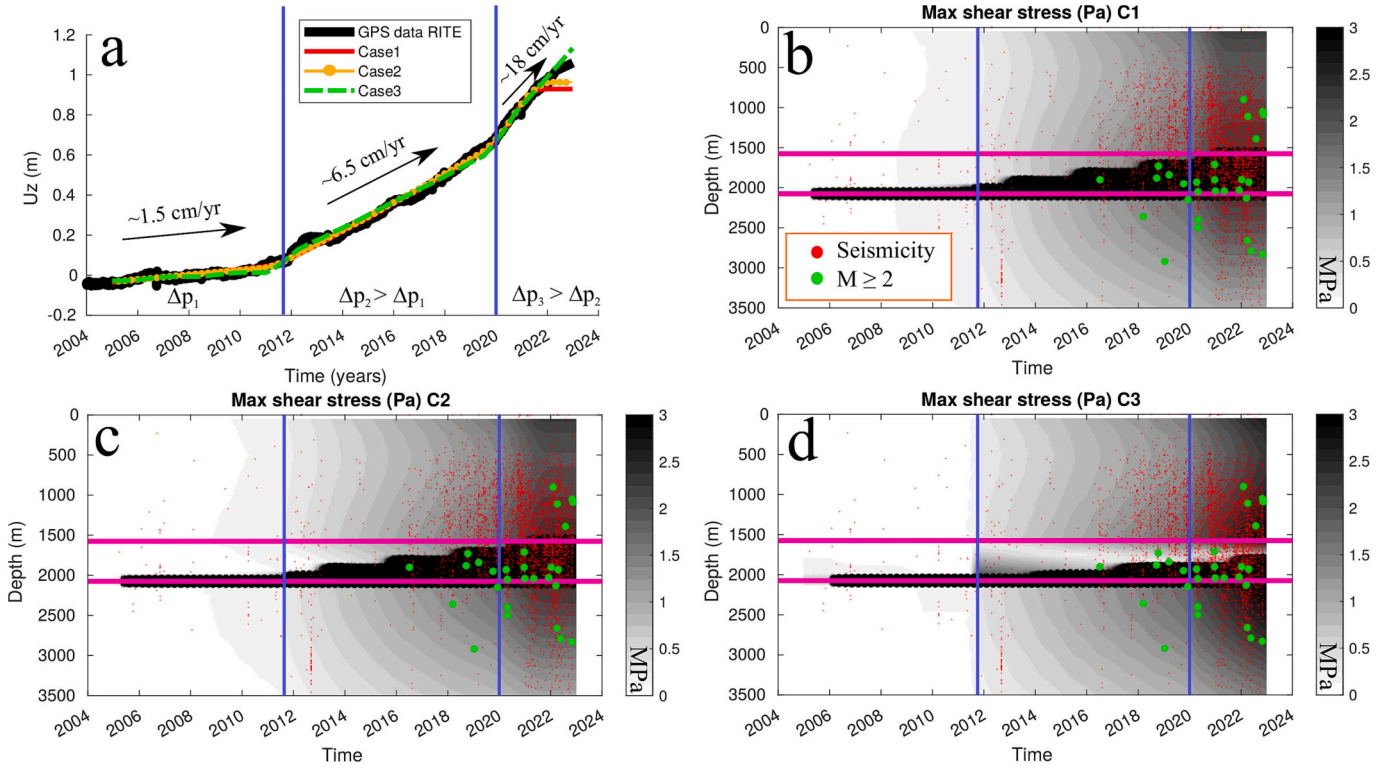

Fig. 4. (a) Uplift measured (black curve) at the RITE CGNSS station (De Martino et al., 2021) and modelled in the 3 different cases C1 to C3. Blue vertical lines indicate the 06/2011 and 01/2020 times. Panels b-d show the maximum shear stress induced by the TPE inclusion, below the RITE station, as a function of time and depth, for the 3 different cases. Red points represent hypocenter locations. Green circles represent the hypocenters of M ≥ 2 events. Magenta lines show the top and bottom boundaries of the TPE inclusion. (For interpretation of the references to colour in this figure legend, the reader is referred to the web version of this article.)

Probability Density Distribution, PPD (e.g. Sambridge, 1999). For the resulting values of pore-pressure and temperature changes at the base of the inclusion (see Fig. 5 for cases C1–3), eqs. (3) and (6) provide an almost constant uplift rate in cases C1–3 (Fig. 4a).

According to (1), both changes in temperature ΔT and pore-pressure Δp influence the magnitude of the displacement, even if the effects of the latter are smaller for reasonable values of parameters H and α_s (Belardinelli et al., 2022; Wang, 2017). This means that, at a given time, the magnitude of the uplift induced by the TPE inclusion is mainly influenced by the temperature changes. Nevertheless, we recall that pore-pressure changes are still very important, because they act on the uplift rate, making the ascent of the advective thermal front slower or faster. The resulting uplift rates are similar in all cases (Fig. 4), indicating that, regardless of the permeability value, there is always a combination of Δp and ΔT (Fig. 5) which is able to reproduce the recorded uplift as a function of time with the same accuracy. This is also due to the fact that there is a crosstalk between the pore-pressure values and the permeability values, according to (5). However, this does not mean that all the results are reasonable. The C4 case, with the lowest permeability, leads to very high Δp_s (>50 MPa) and ΔT (>1000 K) therefore we discarded it, for the reasons that will be given in the next section.

The maximum shear stress, in all cases, is significant (from 10^5 to 10^7 Pa) and is characterized by a progressive increment over time, both within and outside the inclusion (Figs. 3b and d). The progressive increment of the maximum shear stress is accompanied by the increment of seismicity with time. The stress reaches its maximum near the bottom of the inclusion, below the thermal front. The thermal front is faster for greater values of permeability (C1). Fig. 6 shows vertical sections of maximum shear stress obtained in C2 at different times (2006, 2012 and 2021). Most of the shear stress is induced inside, at the bottom of the TPE inclusion and below the thermal front. A significant shear stress is also induced near the lateral boundary of the inclusion. The compressional axis of stress is vertical and compatible with extensional environments in the whole domain, apart from a thinner layer inside the inclusion, below the thermal front, where a horizontally compressional environment is induced. Accordingly, during the entire process, the number of favoured normal earthquakes is expected to be much larger than the one of thrust earthquakes.

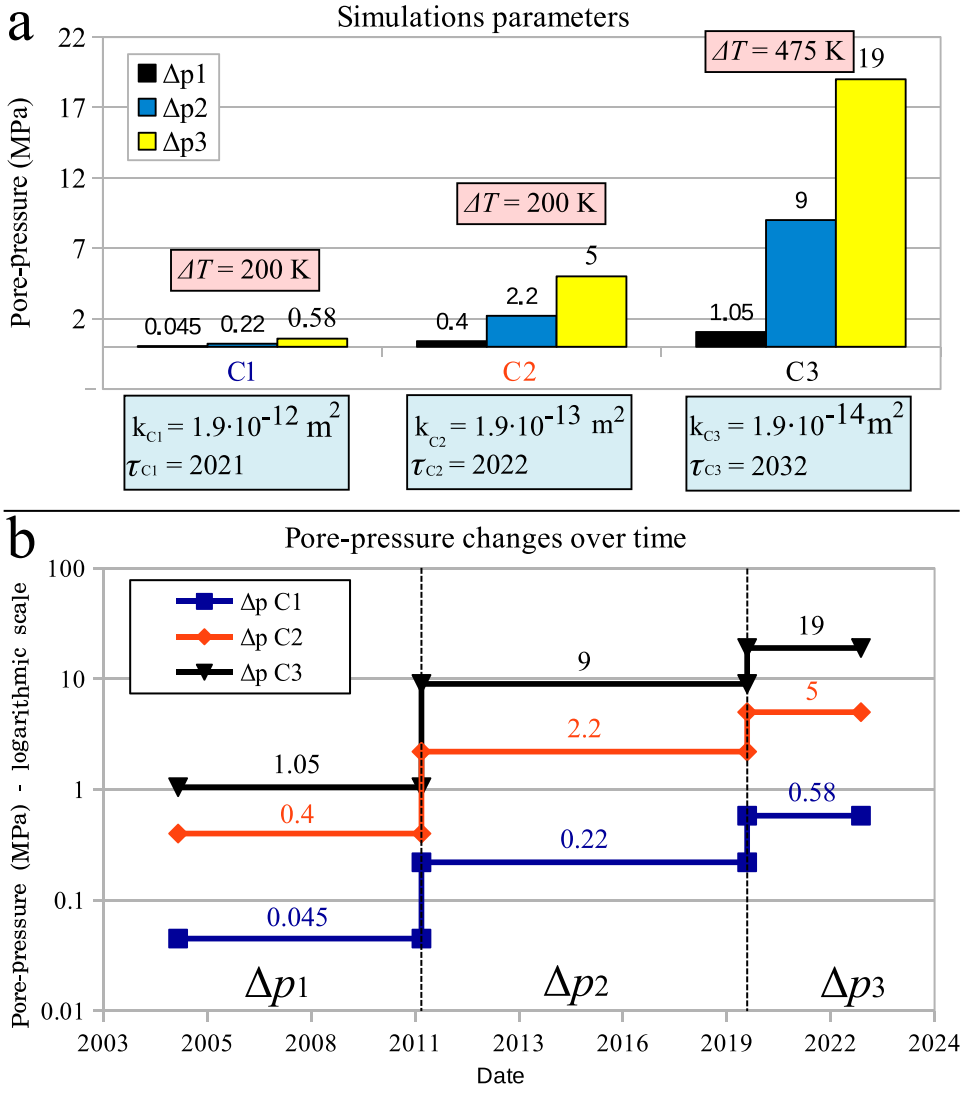

Fig. 5. (a) Pore pressure and temperature changes estimated for the cases C1, C2 and C3 with different permeabilities (k_{C1}, k_{C2} and k_{C3}). Δp_1 (black), Δp_2 (blue) and Δp_3 (yellow) are the pore pressure values estimated at the base of the TPE inclusion during the three different time windows. ΔT is the temperature change estimated at the base of the TPE inclusion starting from 2005, while τ_{C1}, τ_{C2} and τ_{C3} are the years in which the temperature front reaches the top of the TPE inclusion. (b) Time series of Δp estimated for the three different cases C1–3, plotted in a logarithmic scale. (For interpretation of the references to colour in this figure legend, the reader is referred to the web version of this article.)

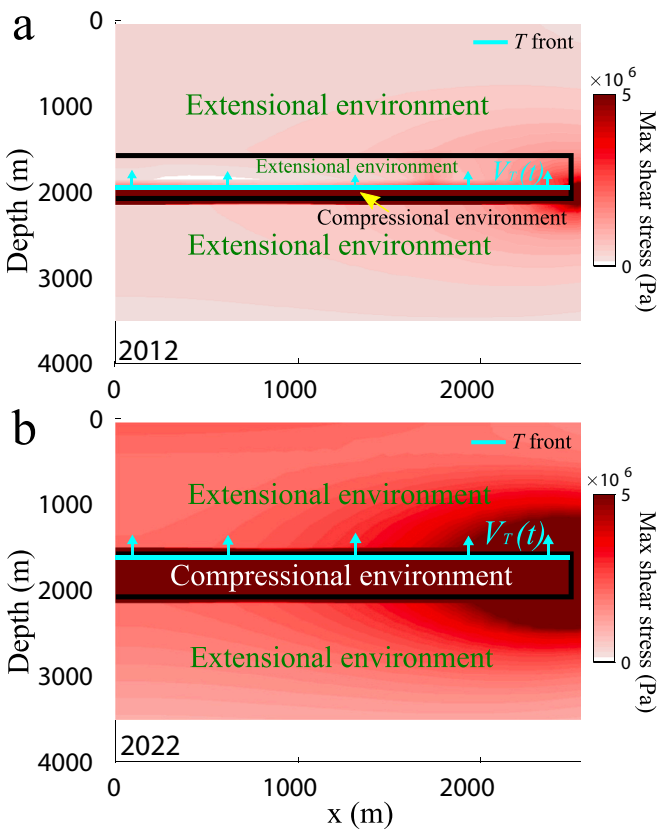

Fig. 6. Vertical sections of maximum shear stress (colour) generated by the TPE inclusion in Case C2 in 2012 (a) and 2022 (b). The black box represents the inclusion boundaries. In the figure also the zones in which extensional or compressional environments are favoured by the TPE inclusion are shown. The light blue lines represent the location of the temperature front which rises toward the top of the inclusion with a speed $V_T(t)$. (For interpretation of the references to colour in this figure legend, the reader is referred to the web version of this article.)

4. Discussion

The b-value anomalies are usually interpreted in terms of material heterogeneity, effective shear stress and/or temperature variations (e.g. Wyss et al., 1997; Wiemer and Wyss, 2002; Schorlemmer et al., 2005). Mapping of b-values reveals the regions, with high b-values, where the production of small earthquakes statistically differs from the average. Different studies conducted in volcanic regions (e.g. Murru et al., 2005; Wyss et al., 2001 and Wiemer and Wyss, 2002) identified areas with an anomalously high b-value, interpreted as partially melted zones embedded within a normal crust. The b-value usually decreases with depth due the increment in the lithostatic pressure. Nevertheless, thermal and/or rheological heterogeneities could result in anomalies of this trend. A decrease in the b-value with depth during the 1982–84 bradiseismic crisis was reported by Vilardo et al. (1991) using the least-square linear regression to fit the Gutenberg-Richter law in the magnitude range 1.2–2.9. A decrement is expected due to the increment in the stress with depth; otherwise in volcanic areas high variations in b are sometimes reported (e.g. Murru et al., 2005). A variation in space of the b-value was described by D' Auria et al. (2011) who evidenced a very low value (~0.5) for the earthquakes that occurred offshore in the 1982–84 period. The sharp decrease in the b-value that we evidenced between 1.5 and 2 km can be associated with the presence of a caprock where the stress can be accumulated. Most of the recent seismicity at Campi Flegrei occurs above 2 km where the presence of the hydrothermal system likely lubricates the faults and fractures which are dense in the area (Tramelli et al., 2022; Selva et al., 2012) and triggers lots of small magnitude events.

Differently from previous applications of TPE inclusion models, which provided static deformation patterns, our approach allowed us to model transient effects of the displacement and seismicity. All the 4 simulations (C1 to C4) presented in the previous section can represent the time-series of the recent uplift observed in the Caldera of Campi Flegrei with a good accuracy because there is always a combination of parameters (Δp and ΔT) that allows us to fit the curve of uplift. Nevertheless, in cases C1, C2 and C3, the range of admissible parameters is quite wide as Δp_1 spans from about 0.05 to 1 MPa, Δp_2 from 0.2 to 9 MPa, Δp_3 from 0.6 to 20 MPa and ΔT from 200 to 475 °C (Fig. 5). These results allow us to assess that TPE effects induced by the inclusion can easily justify both the magnitude of the displacement and its corresponding uplift rate. The parametric test performed by assuming different permeability values is necessary, since the range of admissible permeability values at Campi Flegrei is constrained by in-situ measurements with large uncertainties (Heap et al., 2014; Carlino et al., 2018). Although our approach does not allow us to identify unique values of p and T inside the inclusion, it allows us to identify admissible intervals of their values, which can effectively explain the deformation observed on the surface. The discussion on the reasonableness of the intervals found, based on the comparison with independent evidence, is made in the following paragraph. It is worth to recall that T and p appearing in (3) and (6) denote changes computed with respect to an initial reference state. In our case, for the sake of simplicity, we can assume that before the fluid exsolution, within the TPE inclusion there was a hydrostatic pore pressure gradient and a uniform temperature. The initial reference state does not affect simulations as according to (1) mechanical effects only depend on p and T changes with respect to an arbitrary reference configuration.

The orders of magnitude $\Delta T \approx 10^2$ K and Δp up to 10^1 MPa can be realistically assumed at the base of the TPE inclusion (Nespoli et al., 2021). Indeed, near magma reservoirs, the temperature is generally greater than typical crustal values and the release of volatiles occurs at near-lithostatic pressures. Moreover, as the mechanical strength of basaltic rocks is generally evaluated in the order of 10^1 MPa (e.g. Heap et al., 2021), it is reasonable to assume that Δp can be up to this value, in order to avoid hydrofracture (e.g. Belardinelli et al., 2022). Such values are also in agreement with geochemical models which indicate that temperature of geothermal fluids in the shallow hydrothermal system of the caldera are usually between 150 and 300 °C and the pore-pressure is up to about 8 MPa (e.g. Carlino et al., 2012; Chiodini et al., 2011, 2021). Taking into account the condition for CH_4 formation, temperatures larger than 360 °C are expected below 2 km of depth (Caliro et al., 2007), while the temperature measured at about 3 km of depth during deep drilling at Campi Flegrei is 420 °C (e.g., de Lorenzo et al., 2001; Piochi et al., 2021; AGIP, 1987). Moreover, according the numerical simulations performed by Afanasyev et al. (2015) the fluid mixture injected from a deep magmatic source at 5 km of depth has a temperature of ~700 °C. Following these independent evidences, we believe that both the Δp (>50 MPa) and the ΔT (>1000 K) achieved by C4 are too high to realistically describe the recent behaviour of Campi Flegrei. Moreover, due to the high permeability assumed in the C1 simulation, the thermal front would have reached the top of the TPE inclusion in 2021 (Fig. 5), without justifying the further ground uplift that is still occurring. These considerations allow us to infer that the smaller values of permeability assumed in C2 and C3 are more suitable to explain the ongoing uplift, suggesting as realistic for permeability the range $\approx 10^{-14}$–10^{-13} m^2. These values are consistent with the measures from boreholes (Piochi et al., 2014; Carlino et al., 2018) and assumed in other independent models (e.g. Todesco, 2009). We could have other constraints on the "heating rate" of the TPE inclusion by observing the future developments of the current unrest phase.

The maximum shear stress generated inside and outside the inclusion (Fig. 4) is significant (up to tens of MPa) and all the analysed cases show

that the TPE inclusion is highly capable of inducing and/or favouring earthquakes. The largest shear stress is generated at the bottom of the inclusion, where *T* is the highest, and it progressively rises in magnitude during time. Since the shear stress is higher below the temperature front, which rises inside the inclusion, the simulations also indicate a progressive increase of the shear stress close to the top of the inclusion. In any case, the increment in shear stress is accompanied by an increase of the seismicity rate. Interestingly, the largest earthquakes ($M \geq 2$) are focused on depths compatible with those of the TPE inclusion, where the model predicts the maximum shear stress (Fig. 4). Furthermore, above the inclusion, where the induced maximum shear stress is lower, the $M \geq 2$ earthquakes start occurring only after 2022, in agreement with the fact that our model predicts an increase of shear stress over time, even outside the inclusion. The direction of compressive stresses induced by the TPE inclusion, during the exsolution of magmatic fluids is generally vertical in all the domain, leading to extensional environments (Fig. 6) with the exception of a narrow volume located inside the inclusion, below the thermal front. This means that during the simulations mostly normal faults are favoured in the overall domain. This is in agreement with the seismicity observed in this recent unrest which is characterized by normal earthquakes (La Rocca and Galluzzo, 2019). As the simulation time progresses, thrust earthquakes can also be favoured within a larger portion of the inclusion. The unrest phase of 1982–1984 was also mainly characterized by normal fault mechanisms. In such a period, however, a non-negligible number of thrust earthquakes were also observed (e.g. D'Auria et al., 2014; Mantiloni et al., 2020; Orsi et al., 1999). It is worth to notice that the simple geometry assumed to represent the TPE inclusion is obviously an approximation (albeit reasonable) of the actual shape of the deformation source. The focal mechanisms depend also on the geometry of the inclusion (Nespoli et al., 2021). A cylindrical TPE inclusion was recently used to model the observed deformation at the Vulcano Island, Italy, by Stissi et al. (2023).

The difference between the 82–84 unrest and the current one (2005-today) could be explained by the different speed of the rising thermal front within the inclusion. In the 82–84 unrest the maximum uplift of about 1.8 m was achieved in just 2 years with a rate of about 1 m/yr. In the current phase, the uplift is increasing (Fig. 4) with a much lower rate: 1–2 cm/yr until ≈2012; 6–7 cm/yr in the period 2012–2020 and about 18 cm/yr in the period 2020–2022. According to our results, the speed of the thermal front within the inclusion (V_T) is linearly dependent on Δp, the change of the pore pressure of the hydrothermal fluids at the base of the TPE inclusion (eq. 4 and 5). We could therefore speculate that the pore pressures of the exsolved fluids during the unrest phase of '82–84 were higher than the ones of the current phase, even if Nespoli et al. (2021) suggested that a significant fraction of the observed deformation should be also ascribed to the inflation of the underlying magma reservoir.

We must clarify that our model hinges on several simplifications. One of the major simplifications is due to the representation of the fluid. Even if our equations are based on 12 different parameters for the description of the fluid-rock interaction, our model neglects the eventual phase changes that could occur during the migration of fluids within the inclusion. The latter can enhance or reduce the temperature changes as due to the release or absorption of latent heat, respectively. Furthermore, our model does not take into account the coupling between pore-pressure and permeability (e.g. Zencher et al., 2006, Rinaldi and Nespoli, 2017), while we are assuming a constant permeability of the medium during the entire process of fluid exsolution. If we consider that the permeability increases due to an increase of pore pressure, the propagation of the fluid would be faster than currently predicted by our model. Our model also neglects the 3D heterogeneities of the medium (e.g. De Siena et al., 2010) and the presence of further deformation sources, nor does it account for the presence of regional, NNE-SSW extensional (D'Auria et al., 2014) tectonic stresses, the effects of which could be superimposed to the one of the TPE inclusion. Nevertheless, the results shown in Fig. 6 should not be significantly affected by the presence of the regional stress field which is expected to be weaker than the stress due to the TPE source (D'Auria et al., 2014), at least in those near field regions where seismicity occurs (Fig. 1). Nespoli et al. (2021) suggested that in order to model the unrest of 82–84, the deformation induced by the inflation of a deep magma chamber should be also taken into consideration in addition to TPE effects. In fact, the mechanical effects of the TPE inclusion should be added to the ones induced by other, deeper, magmatic deformation sources (e.g. Bonafede et al., 1986; Trasatti et al., 2011, 2015). The presence of a deep magmatic deformation source could justify the occurrence of some significant earthquakes ($M \geq 2$) in the deeper part of the caldera (Fig. 1). An interesting improvement of the applied method would be to study the combined effect of the two different sources of deformation (TPE and magmatic). A further advancement of the work could consist in reproducing the subsidence phases, that generally follow the uplift episodes, in terms of depressurization and cooling of the TPE inclusion. Another improvement to the model could be to consider the viscoelastic effects of the rocks (Nespoli et al., 2023). Part of the simplifications assumed in our model could be treated in the future, probably with the help of more realistic (and complex) numerical models. However, the latter must be validated by an analytical background.

5. Conclusions

The simulations presented in this work give significant insights into the understanding of the physics that regulates the TPE behaviour within a hydrothermal system. Differently from previous applications we employed a TPE deformation source to model the transient effects due to the propagation of fluids within it. The results confirm that our TPE model allows us to effectively explain both the uplift rate and the trend of the seismicity. The presence of the modelled TPE volume at Campi Flegrei is supported by the analysis of the b-values which has a sharp variation below 1.5 km of depth, corresponding to the depth of the top of the TPE inclusion. Below 1.5 km, the TPE inclusion-induced shear stress is maximum, and the occurrence of the largest earthquakes is expected justifying the sharp decrease of the b-values. We are confident that the results presented in this work can broaden the debate in terms of geohazards for the Campi Flegrei caldera. This is primally true, at the time we are writing, because the yellow state of alert has been issued for the studied area since 2012. Even if the TPE model is here applied to the caldera of Campi Flegrei, it can certainly find an appropriate application in other volcanic or geothermal areas as well. Finally, thermo-fluid dynamical effects might be invoked also during the uprise of highly viscous magmatic fluids, since even in this case we face heat advection through mass movement promoted by a pressure gradient. However in this case the main mechanism of magma uprise is generally ascribed to the upward propagation of tensile fractures (dike opening), a process that cannot be described by Darcy law and would request a completely different approach.

Author statement

Massimo Nespoli (conceptualization, formal analysis, methodology, software, visualization, writing original draft), Anna Tramelli (conceptualization, formal analysis, methodology, software, visualization, writing original draft), Maria Elina Belardinelli (conceptualization, methodology, validation, writing-review and editing), Maurizio Bonafede (conceptualization, methodology, validation, writing-review and editing).

Declaration of Competing Interest

The authors declare that they have no known competing financial interests or personal relationships that could have appeared to influence the work reported in this paper.

Data availability

The seismic catalog can be downloaded from https://doi.org/10.5281/zenodo.7961857.

Acknowledgements

The authors would like to thank the Editor Diana Roman and the reviewers Maurizio Battaglia and Freysteinn Sigmundsson for helpful comments and useful discussions.

References

Afanasyev, A., Costa, A., Chiodini, G., 2015. Investigation of hydrothermal activity at Campi Flegrei caldera using 3D numerical simulations: extension to high temperature processes. J. Volcanol. Geotherm. Res. 299, 68–77. ISSN 0377–0273. https://doi.org/10.1016/j.jvolgeores.2015.04.004.

AGIP, 1987. Geologia e Geofisica del Sistema Geotermico dei Campi Flegrei. Servizi Centrali per l'Esplorazione, SERGMMESG, San Donato, p. 19.

Aki, K., 1965. Maximum likelihood estimate of b in the formula log N = a − bM and its confidence limits. Bull. Earthquake Res. Inst. Tokyo Univ. 43, 237–239.

Aki, K., Richards, P.G., 2002. Quantitative seismology, 2nd edition, 1. University Science Books.

Amoruso, A., Crescentini, L., Linde, A.T., Sacks, I.S., Scarpa, R., Romano, P., 2007. A horizontal crack in a layered structure satisfies deformation for the 2004–2006 uplift of Campi Flegrei. Geophys. Res. Lett. 34, L22313. https://doi.org/10.1029/2007GL031644.

Amoruso, A., Crescentini, L., Sabbetta, I., 2014. Paired deformation sources of the Campi Flegrei caldera (Italy) required by recent (1980–2010) deformation history. J. Geophys. Res. Solid Earth 119, 858–879. https://doi.org/10.1002/2013JB010392.

Battaglia, M., Troise, C., Obrizzo, F., Pingue, F., Natale, G.D., 2006. Evidence for fluid migration as the source of deformation at Campi Flegrei caldera (Italy). Geophys. Res. Lett. 33 (1) https://doi.org/10.1029/2005GL024904.

Bejan, A., 1984. Convection Heat Transfer. Wiley.

Belardinelli, M., Bonafede, M., Nespoli, M., 2019. Stress heterogeneities and failure mechanisms induced by temperature and pore-pressure increase in volcanic regions. Earth Planet. Sci. Lett. 525, 115765. https://doi.org/10.1016/j.epsl.2019.115765.

Belardinelli, M.E., Nespoli, M., Bonafede, M., 2022. Stress changes caused by exsolution of magmatic fluids within an axi-symmetric inclusion. Geophys. J. Int. Ggac093 https://doi.org/10.1093/gji/ggac093. URL.

Benussi, C., Belardinelli, M.E., Nespoli, M., 2023. How to model thick thermo-poro-elastic inclusions. Bull. Geophys. Oceanogr. https://doi.org/10.4430/bgo00429.

Berrino, G., 1994. Gravity changes induced by height-mass variations at the Campi Flegrei caldera. J. Volcanol. Geotherm. Res. 61 (3), 293–309. https://doi.org/10.1016/0377-0273(94)90010-8. International Conference on Active Volcanoes and Risk Mitigation. URL. http://www.sciencedirect.com/science/article/pii/0377027394900108.

Bevilacqua, A., De Martino, P., Giudicepietro, F., et al., 2022. Data analysis of the unsteadily accelerating GPS and seismic records at Campi Flegrei caldera from 2000 to 2020. Sci. Rep. 12, 19175. https://doi.org/10.1038/s41598-022-23628-5.

Bianco, F., Del Pezzo, E., Saccorotti, G., Ventura, G., 2004. The role of hydrothermal fluids in triggering the July August 2000 seismic swarm at Campi Flegrei, Italy: evidence from seismological and mesostructural data. J. Volcanol. Geotherm. Res. 133 (1–4), 229–246. https://doi.org/10.1016/S0377-0273(03)00400-1.

Biot, M.A., 1941. General theory of three-dimensional consolidation. J. Appl. Phys. 12 (2), 155–164.

Bonafede, M., Dragoni, M., Quareni, F., 1986. Displacement and stress fields produced by a Centre of dilation and by a pressure source in a viscoelastic half-space: Application to the study of ground deformation and seismic activity at campi flegrei, Italy. Geophys. J. R. Astron. Soc. 87 (2), 455–485.

Caliro, S., Chiodini, G., Moretti, R., Avino, R., Granieri, D., Russo, M., Fiebig, J., 2007. The origin of the fumaroles of la solfatara (Campi Flegrei, South Italy). Geochim. Cosmochim. Acta 71 (12), 3040–3055. https://doi.org/10.1016/j.gca.2007.04.007.

Calò, M., Tramelli, A., 2018. Anatomy of the Campi Flegrei caldera using enhanced seismic tomography models. Sci. Rep. 8 (16254) https://doi.org/10.1038/s41598-018-34456-x.

Carlino, S., Somma, R., Troise, C., Natale, G.D., 2012. The geothermal exploration of campanian volca- noes: Historical review and future development. Renew. Sust. Energ. Rev. 16 (1), 1004–1030. https://doi.org/10.1016/j.rser.2011.09.023.

Carlino, S., Piochi, Monica, Tramelli, Anna, Mormone, Angela, Montanaro, Cristian, Scheu, Bettina, Klaus, Mayer, 2018. Field-scale permeability and temperature of volcanic crust from borehole data: Campi Flegrei, southern Italy. J. Volcanol. Geotherm. Res. 357, 276–286. ISSN 0377–0273. https://doi.org/10.1016/j.jvolgeores.2018.05.003.

Chiodini, G., Avino, R., Caliro, S., Minopoli, C., 2011. Temperature and pressure gas geoindicators at the solfatara fumaroles (campi flegrei)'. Ann. Geophys. 54, 2. https://doi.org/10.4401/ag-5002, URL: http://hdl.handle.net/2122/7211.

Chiodini, G., Vandemeulebrouck, J., Caliro, S., D'Auria, L., De Martino, P., Mangiacapra, A., Petrillo, Z., 2015. Evidence of thermal-driven processes triggering the 20052014 unrest at campi flegrei caldera. Earth Planet. Sci. Lett. 414, 58–67. URL: https://www.sciencedirect.com/science/article/pii/S0012821X15000333.

Chiodini, G., Caliro, S., Avino, R., Bini, G., Giudicepietro, F., De Cesare, W., Ricciolino, P., Aiuppa, A., Cardellini, C., Petrillo, Z., Selva, J., Siniscalchi, A., Tripaldi, S., 2021. Hydrothermal pressure-temperature control on CO_2 emissions and seismicity at Campi Flegrei (Italy). J. Volcanol. Geotherm. Res. 414, 107245. https://doi.org/10.1016/j.epsl.2015.01.012.

D'Auria, L., Martini, M., Esposito, A., Ricciolino, P., Giudicepietro, F., 2008. A unified 3D velocity model for the Neapolitan volcanic areas. In: Marzocchi, W., Zollo, A. (Eds.), Conception, Verification and Application of Innovative Techniques to Study Active Volcanoes. INGV-DPC, Naples, Italy, pp. 375–390.

D' Auria, L., Giudicepietro, F., Aquino, I., Borriello, G., Del Gaudio, C., Lo Bascio, D., Ricco, C., 2011. Repeated fluid-transfer episodes as a mechanism for the recent dynamics of Campi Flegrei caldera (1989–2010). J. Geophys. Res. Solid Earth 116 (B4). https://doi.org/10.1029/2010JB007837.

D'Auria, L., Pepe, S., Castaldo, R., et al., 2015. Magma injection beneath the urban area of Naples: a new mechanism for the 2012–2013 volcanic unrest at Campi Flegrei caldera. Sci Rep 5, 13100. https://doi.org/10.1038/srep13100.

De Martino, P., Dolce, M., Brandi, G., Scarpato, G., Tammaro, U., 2021. The Ground Deformation History of the Neapolitan Volcanic Area (Campi Flegrei Caldera, Somma–Vesuvius Volcano, and Ischia Island) from 20 Years of Continuous GPS Observations (2000–2019). Remote Sens. 13 (14), 2725. https://doi.org/10.3390/rs13142725.

De Natale, G., Troise, C., Pingue, F., 2001. A mechanical fluid-dynamical model for ground movements at Campi Flegrei caldera. J. Geodyn. 32, 487–517. https://doi.org/10.1016/S0264-3707(01)00045-X.

De Siena, L., Del Pezzo, E., Bianco, F., 2010. Seismic attenuation imaging of Campi Flegrei: evidence of gas reservoirs, hydrothermal basins, and feeding systems. J. Geophys. Res. 115, B09312. https://doi.org/10.1029/2009JB006938.

De Vivo, B., 2006. Volcanism in the Campania Plain: Vesuvius, Campi Flegrei and Ignimbrites, Vol. 9. Elsevier.

Di Vito, M.A., Isaia, R., Orsi, G., Southon, J.D., Vita, S.D., d'Antonio, M., Pappalardo, L., Piochi, M., 1999. Volcanism and deformation since 12,000 years at the Campi Flegrei caldera (Italy). J. Volcanol. Geotherm. Res. 91 (2–4), 221–246. https://doi.org/10.1016/S0377-0273(99)00037-2.

Eshelby, J.D., 1957. The determination of the elastic field of an ellipsoidal inclusion, and related problems. Proc. R. Soc. Lond. A 241 (1226), 376–396.

Heap, M.J., Baud, P., Meredith, P.G., Vinciguerra, S., Reuschlé, T., 2014. The permeability and elastic moduli of tuff from Campi Flegrei, Italy: implications for ground deformation modelling. Solid Earth 5, 25–44. https://doi.org/10.5194/se-5-25-2014.

Heap, M.J., Wadsworth, F.B., Heng, Z., Xu, T., Griffiths, L., Aguilar Velasco, A., Vair, E., Vistour, M., Reuschl, T., Troll, V.R., Deegan, F.M., Tang, C., 2021. The tensile strength of volcanic rocks: experiments and models. J. Volcanol. Geotherm. Res. 418, 107348. https://doi.org/10.1016/j.jvolgeores.2022.107576.

Judenherc, S., Zollo, A., 2004. The bay of Naples (southern Italy): Constraints on the volcanic structures inferred from a dense seismic survey. J. Geophys. Res. Solid Earth 109 (B10). https://doi.org/10.1029/2003JB002876.

La Rocca, M., Galluzzo, D., 2019. Focal mechanisms of recent seismicity at Campi Flegrei, Italy. J. Volcanol. Geotherm. Res. 388, 106687. https://doi.org/10.1016/j.jvolgeores.2019.106687.

Lima, A., PBodnar, R.J., De Vivo, B., Spera, F., Belkin, H., 2021. Interpretation of recent unrest events (bradyseism) at Campi Flegrei, Napoli (Italy): Comparison of models based on cyclical hydrothermal events versus shallow magmatic intrusive events. Geofluids 1–16. https://doi.org/10.1155/2021/2000255.

D'Auria, L., Massa, B., Cristiano, E., Gaudio, C.D., Giudicepietro, F., Ricciardi, G., Ricco, C., 2014. Retrieving the stress field within the Campi Flegrei caldera (southern Italy) through an integrated geodetical and seismological approach. Pure Appl. Geophys. 172 (11), 3247–3263. https://doi.org/10.1007/s00024-014-1004-7.

de Lorenzo, S., Gasparini, P., Mongelli, F., Zollo, A., 2001. Thermal state of the Campi Flegrei caldera inferred from seismic attenuation tomography. J. Geodyn. 32, 467–486. https://doi.org/10.1016/S0264-3707(01)00044-8.

Mantiloni, L., Nespoli, M., Belardinelli, M.E., Bonafede, M., 2020. Deformation and stress in hydrothermal regions: the case of a disk-shaped inclusion in a half-space. J. Volcanol. Geotherm. Res. 403, 107011. https://doi.org/10.1016/j.jvolgeores.2020.107011.

McTigue, D.F., 1986. Thermoelastic response of fluid-saturated porous rock. J. Geophys. Res. 91 (B9), 9533–9542.

Murru, M., Montuori, C., Console, R., Lisi, A., 2005. Mapping of the b value anomalies beneath Mt. Etna, Italy, during July–August 2001 lateral eruption. Geophys. Res. Lett. 32 (5) https://doi.org/10.1029/2004GL021545.

Nespoli, M., Belardinelli, M.E., Bonafede, M., 2021. Stress and deformation induced in layered media by cylindrical thermo-poro-elastic sources: an application to campi flegrei (Italy). J. Volcanol. Geotherm. Res. 415, 107269. https://doi.org/10.1016/j.jvolgeores.2021.107269.

Nespoli, M., Belardinelli, M.E., Cal, M., Tramelli, A., Bonafede, M., 2022. Deformation induced by distributions of single forces in a layered half-space. EFGRN/EFCMP. Comput. Geosci. 164, 105136. https://doi.org/10.1016/j.cageo.2022.105136.

Nespoli, M., Belardinelli, M.E., Bonafede, M., 2023. Thermo-poro-viscoelastic response of a disc-shaped inclusion. Geophys. J. Int. 235, 135–149. https://doi.org/10.1093/gji/ggad212.

Orsi, G., Civetta, L., Del Gaudio, C., de Vita, S., Di Vito, M., Isaia, R., Petrazzuoli, S., Ricciardi, G., Ricco, C., 1999. Short-term ground deformations and seismicity in the resurgent Campi Flegrei caldera (Italy): an example of active block-resurgence in a densely populated area. J. Volcanol. Geotherm. Res. 91 (2), 415–451. https://doi.org/10.1016/S0377-0273(99)00050-5.

Piochi, M., Kilburn, C.R.J., Di Vito, M.A., et al., 2014. The volcanic and geothermally active Campi Flegrei caldera (2014): an integrated multidisciplinary image of its

buried structure. Int. J. Earth Sci. (Geol. Rundsch.) 103, 401–421. https://doi.org/10.1007/s00531-013-0972-7.
Piochi, M., Cantucci, B., Montegrossi, G., Currenti, G., 2021. Hydrothermal alteration at the san vito area of the campi flegrei geothermal system in Italy: mineral review and geochemical modeling. Minerals 2021 (11), 810. https://doi.org/10.3390/min11080810.
Rinaldi, A.P., Nespoli, M., 2017. TOUGH2-SEED: A coupled fluid flow and mechanical-stochastic approach to model injection-induced seismicity. Comput. Geosci. 108, 86–97. https://doi.org/10.1016/j.cageo.2016.12.003. TOUGH Symposium 2015: Recent Enhancements to the TOUGH Family of Codes and Coupled Flow and Geomechanics Processes Modeling.
Sambridge, M., 1999. Geophysical inversion with a neighbourhood algorithm-II. Apprais-ing the ensemble. Geophys. J. Int. 138 (3), 727–746. https://doi.org/10.1046/j.1365-246X.1999.00876.x.
Schorlemmer, D., Wiemer, S., Wyss, M., 2005. Variations in earthquake-size distribution across different stress regimes. Nature 437, 539–542. https://doi.org/10.1038/nature04094.
Selva, J., Orsi, G., Di Vito, M.A., Marzocchi, W., Sandri, L., 2012. Probability hazard map for future vent opening at the Campi Flegrei caldera, Italy. Bull. Volcanol. 74, 497–510. https://doi.org/10.1007/s00445-011-0528-2.
Shi, Y., Bolt, B.A., 1982. The standard error of the magnitude-frequency b value. Bull. Seismol. Soc. Am. 72 (5), 1677–1687. https://doi.org/10.1785/BSSA0720051677.
Stissi, S.C., Currenti, G.M., Cannavo, F., Napoli, R., 2023. Evidence of poro-elastic inflation at the onset of the 2021 Vulcano Island unrest. Front. Earth Sci. Sec. Volcanol. 11 https://doi.org/10.3389/feart.2023.1179095.
Todesco, M., 2009. Signals from the Campi Flegrei hydrothermal system: Role of a "magmatic" source of fluids. J. Geophys. Res. 114, B05201. https://doi.org/10.1029/2008JB006134.
Todesco, M., 2021. Calderas breathing: Poroelastic ground deformation at campi flegrei (Italy). Front. Earth Sci. 9, 691. URL: https://doi.org/10.3389/feart.2021.702665.
Tramelli, A., Godano, C., Ricciolino, P., Giudicepietro, F., Caliro, S., Orazi, M., De Martino, P., Chiodini, G., 2021. Statistics of seismicity to investigate the campi flegrei caldera unrest. Sci. Rep. 11 (1), 7211. https://doi.org/10.1038/s41598-021-86506-6.
Tramelli, A., Giudicepietro, F., Ricciolino, P., Chiodini, G., 2022. The seismicity of campi flegrei in the contest of an evolving long term unrest. Sci. Rep. 12 (1), 2900. https://doi.org/10.1038/s41598-022-06928-8.
Trasatti, E., Bonafede, M., Ferrari, C., Giunchi, C., Berrino, G., 2011. On deformation sources in volcanic areas: modeling the Campi Flegrei (Italy) 1982–84 unrest. Earth Planet. Sci. Lett. 306 (3–4),, 175–185. https://doi.org/10.1016/j.epsl.2011.03.033.
Trasatti, E., Polcari, M., Bonafede, M., Stramondo, S., 2015. Geodetic constraints to the source mechanism of the 2011–2013 unrest at Campi Flegrei (Italy) caldera. Geophys. Res. Lett. 42 (10), 3847–3854. https://doi.org/10.1002/2015GL063621.
Troiano, A., Di Giuseppe, M.G., Isaia, R., 2022. 3D structure of the Campi Flegrei caldera central sector reconstructed through short-period magnetotelluric imaging. Sci. Rep. 12, 20802. https://doi.org/10.1038/s41598-022-24998-6.
Turcotte, D.L., 1989. Fractals in geology and geophysics. PAGEOPH 131, 171–196. https://doi.org/10.1007/BF00874486.
Vilardo, G., Alessio, G., Luongo, G., 1991. Analysis of the magnitude-frequency distribution for the 19831984 earthquake activity of Campi Flegrei, Italy. J. Volcanol. Geotherm. Res. 48 (1), 115–125. https://doi.org/10.1016/0377-0273(91)90037-Z.
Vitale, S., Natale, J., 2023. Combined volcano-tectonic processes for the drowning of the Roman western coastal settlements at Campi Flegrei (southern Italy). Earth Planets Space 75, 38. https://doi.org/10.1186/s40623-023-01795-7.
Wang, H.F., 2017. Theory of Linear Poroelasticity with Applications to Geomechanics and Hydrogeology. Princeton University Press.
Wiemer, S., Wyss, M., 2002. Mapping spatial variability of the frequency-magnitude distribution of earthquakes. In: Advances in Geophysics, 45. Elsevier, p. 259V. https://doi.org/10.1016/S0065-2687(02)80007-3.
Wyss, M., Klein, F., Nagamine, K., Wiemer, S., 2001. Anomalously high b-values in the South Flank of Kilauea volcano, Hawaii: evidence for the distribution of magma below Kilauea's East rift zone. Journal of Volcanology and Geothermal Research 106 (1–2), 23–37.https. https://doi.org/10.1016/S0377-0273(00)00263-8.
Wyss, M., Shimazaki, K., Wiemer, S., 1997. Mapping active magma chambers by b values beneath the off-Ito volcano, Japan. J. Geophys. Res. Solid Earth 102 (B9), 20413–20422. https://doi.org/10.1029/97JB01074.
Zencher, F., Bonafede, M., Stefansson, R., 2006. Near-lithostatic pore pressure at seismogenic depths: a thermoporoelastic model. Geophys. J. Int. 166 (3), 1318–1334. https://doi.org/10.1111/j.1365-246X.2006.03069.x.